Experiments on the collective acceleration of ions by a relativistic electron cloud

A. V. Burdakov, V. S. Koĭdan, A. I. Rogozin, and V. V. Chikunov

Institute of Nuclear Physics, Siberian Division of the Academy of Sciences of the USSR
(Submitted 6 September 1980)
Zh. Eksp. Teor. Fiz. **80**, 1391–1408 (April 1981)

The results of experiments on the collective acceleration of ions by a relativistic-electron cloud produced near a thin foil upon the injection through it of a supercritical-current-carrying relativistic-electron beam (REB) are presented. The ions are accelerated at the expense of the energy of a cloud of electrons from a plasma produced during the ionization of a hydrogen-containing dielectric film located near the foil anode of the accelerator. The experiments were performed with the following REB parameters: current $I_{max} \approx 20$ kA, electron energy $E_{max} \approx 1$ MeV, pulse duration $\tau \approx 50$ nsec; the longitudinal-magnetic-field strength $H_0 \lesssim 20$ kOe. The ion-acceleration regime that is optimal with respect to the transfer of energy from the REB to the ion flux has been found. The acceleration efficiency in the optimal regime attains a value $\sim 50\%$. The total number of accelerated protons is equal to 2×10^{15} per pulse. The highest proton current is ~ 3.5 kA for a current density of ~ 400 A/cm^2. It is shown that most of the electrons have energies $\lesssim 1$ MeV, but some of them are accelerated to energies significantly higher than the energy of the REB electrons. It is found that the accelerated flux contains, besides protons, carbon ions, H_2^+ ions, and hydrogen atoms.

PACS numbers: 41.80.Gg, 29.15. – n

I. INTRODUCTION

It is now theoretically[1,2] and experimentally[3] established that the injection of a supercritical-current-carrying high-power relativistic-electron beam (REB) into the vacuum of an accelerator causes the formation near the accelerator's foil anode of a cloud of oscillating electrons whose density may be higher than that of the initial beam by a factor of several tens. One of the possible applications of such a cloud is the use of the energy stored in it for the collective acceleration of ions.[4]

The principle of ion acceleration by an electron cloud consists in the following (Fig. 1). A REB with current significantly higher then the critical vacuum current is produced in a high-current diode consisting of a cathode 1 and a thin conducting foil 2. The diode and the vacuum drift chamber are located in a longitudinal magnetic field H_0. Under such conditions the majority of the electrons injected into the chamber are reflected, and begin to oscillate between the cathode and the "virtual cathode" that arises in the drift chamber behind the foil anode. As a result, a cloud of oscillating electrons is formed near the foil 2. Under certain conditions the oscillating electrons can produce near the surface of the foil anode (through the ionization of the dielectric film 3, for example) a plasma layer that serves as an ion source. Under the action of the electric field of the electron cloud, the ions, leave this plasma, and, neutralizing the space charge of the oscillating electrons, move along the chamber, and thus accelerate. In other words, there is formed a plasma, consisting of ions and oscillating relativistic electrons, that expands along the lines of force of the magnetic field. In the process the electron gas "cools down," transferring its energy to the ions. Ryutov[5] calls this method of collectivity accelerating ions the "gas-dynamical" method, in view of the fact that the equations describing the cloud-expansion process coincide with the equations of one-dimensional gas dynamics. As shown by Ryutov and Stupakov[4] in such an acceleration, the ions can acquire energies comparable to the energy of the injected electrons, and some of them will be accelerated to significantly higher energies. The acceleration efficiency (i.e., the portion of energy transferred from the electron cloud to the ions) in this method of acceleration can, according to Stupakov's theoretical estimates,[6] attain a value of 70%.

A number of other methods of accelerating ions are now being developed (see, for example, Refs. 7–10 for a review), in particular, those in which oscillating electrons are used. Thus, in the reflecting systems described in Refs. 11 and 12, in contrast to the method considered by us here, the anode unit (i.e., the ion emitter) is at a high positive potential with respect to the drift chamber and the cathode, and a "direct" (and not a collective) acceleration of the ions is realized. The electronic component of the bipolar current of the diode in these systems is strongly suppressed as a result of the fact that the electrons oscillate around the foil anode. In consequence, the ion current can be significantly higher than the value given by the Child–Langmuir law, while the ion energy corresponds to the anode voltage potential. Nevertheless, collective acceleration of at least part of the ion flux can occur in the reflecting systems too.

The actual feasibility of a sufficiently effective collective gas-dynamical acceleration of ions was demonstrated by us.[13,14] In the present paper we present the re-

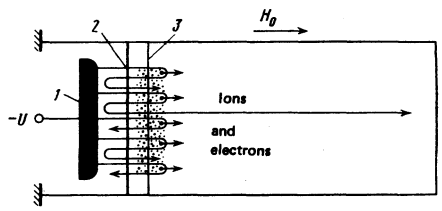

FIG. 1. Scheme of ion acceleration by a relativistic-electron cloud: 1) cathode, 2) foil anode, and 3) dielectric film.

 0038-5646/81/040712-10$02.40

sults of a systematic experimental investigation of this method of acceleration. The primary purpose of the experiments described below was to find the conditions corresponding to the highest acceleration efficiency, as well as to investigate the properties of the generated ion flux.

II. THE EXPERIMENTAL SETUP AND THE MEASUREMENT PROCEDURE

1. The experiments were performed on the "KRAB" facility. A diagram of the setup is shown in Fig. 2. A high-voltage pulse of negative polarity is fed to a graphite cathode, 3, of diameter 3 cm. A relativistic-electron beam is injected through foils, 5 and 6, into a glass vacuum chamber of diameter 11 cm, which was evacuated down to a pressure of 10^{-5} Torr. The accelerator diode and the vacuum chamber were placed in a solenoid with the aid of which a quasistationary longitudinal magnetic field of intensity ≤ 20 kOe was produced.

As the foil anode 5, we used a thin aluminum foil or a dielectric foil with an aluminum coating of thickness $\lesssim 3$ μm. Located behind the foil anode was a dielectric film, 6, which was the ion emitter.[1)] In the experiments on proton acceleration, we used dielectric films prepared from hydrogen-containing materials. For the deuteron acceleration we used a fluoroplastic film of thickness 6 μm, coated with a deuterated polyethylene layer of thickness $\lesssim 10$ μm. To prepare this coating, powdered deuterated polyethylene was first dissolved in hot xylene, and the solution obtained was then applied to the surface of the film, after which the xylene was evaporated.

2. In the experiments we recorded both the electron-beam parameters and the parameters of the accelerated-ion flux. The diode current and the total current flowing in the drift chamber were measured with Rogowski loops 2. The current to the collector 8 was recorded with the aid of a shunt. The voltage potential on the accelerator cathode was measured with the aid of a capacity divider 4.

For the registration of the accelerated-ion-flux parameters, we used both already known methods (see, for example, Ref. 15) and some new diagnostics. In the experiments we extensively used the nuclear diagnostic methods based on the fact that if the energy of the accelerated protons or deuterons exceeds threshold values, then these particles, striking a target prepared from a definite material, are capable of initiating nuclear reactions. The registration of the accelerated particles was carried out with the aid of the products of the following nuclear reactions:

$$^{12}C(d,n)^{13}N(\beta^+)^{13}C,\ ^{12}C(p,\gamma)^{13}N(\beta^+)^{13}C,\ ^{14}N(p,\gamma)^{15}O(\beta^+)^{15}N,$$
$$^{19}F(p,\alpha\gamma)^{16}O,\ ^{10}B(p,\gamma)^{11}C(\beta^+)^{11}B.$$

The half-lives of the isotopes produced and the reaction yields for thick targets have been listed by, for example, Young *et al.*[15] The yield of the reaction $^{12}C(p,\gamma)^{13}N$ depends weakly on the proton energy. Consequently, the number of protons with energy higher than the reaction-threshold energy (i.e., with $E_p > 0.47$ MeV) can easily be determined from the number of radioactive nuclear ^{13}N produced in the carbon target. The yield of the reaction $^{12}C(d,n)^{13}N$ strongly depends on the energy. Therefore, additional information about the energy spectrum of the accelerated deuterons is necessary for the determination of the number of these particles.

The proton flux contains a deuterium-ion impurity, due to the natural presence of deuterium in the hydrogen-containing dielectric film. The additional activation of the target by deuterons was taken into account in the same way as was done in Ref. 15.

The induced activity in the graphite (C) or boron-nitride (BN) targets was measured with the aid of two scintillation counters connected in a coincidence scheme. They registered γ quanta, which were produced as a result of positron annihilation. FÉU-110 photomultipliers with NaI(Tl) crystals were used in the counters. To decrease the number of spurious counts caused by the photomultiplier noise pulses, the signals were amplitude-discriminated before the coincidence circuit.

The irradiation of a target by an intense ion beam can lead to the heating and damage of the target surface, as a result of which some of the radioactive nuclei may be lost.[16,17] It was established with the aid of screens placed in front of the target that the effect of the target damage can be neglected in our experiments.

3. The number of $^{12}C(d,n)^{13}N$ nuclear reactions that occurred in the carbon target was also determined from the neutron yield. The total number of neutrons produced in this reaction was measured by a neutron activation detector. As the radioactive tracer in the detector, we used a silver foil located in a paraffin neutron moderator. The detector had the geometry of a "flat-response" neutron center.[18] Such a geometry ensures the nondependence of the neutron-registration efficiency on the neutron energy. The results of the measurements of the number of nuclear reactions with the aid of a neutron activation detector and the γ-γ-coincidence method agree with each other.[13] This is another confirmation of the fact that appreciable losses of the radioactive ^{13}N nuclei from the target did not occur in our experiments.

4. In individual experiments the ion beam was received

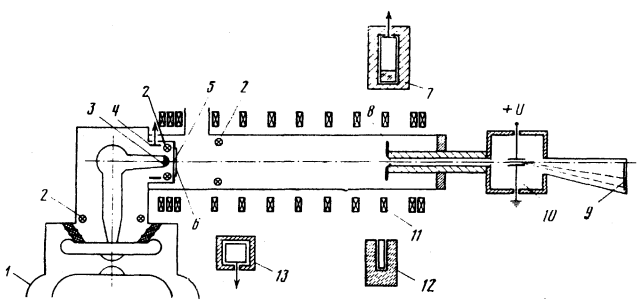

FIG. 2. Diagram of the "KRAB" facility: 1) accelerator, 2) Rogowski loop, 3) cathode, 4) capacity voltage divider, 5) and 6) anode foils, 7) prompt-γ-radiation detector, 8) collector, 9) nuclear photoemulsion, 10) electrostatic analyzer, 11) solenoid, 12) neutron activation detector, 13) time-of-flight neutron detector.

by a graphite collector, which consisted of 45 separate sections. The radial profile of the accelerated-ion beam was studied with the aid of this collector.[13] In the deuteron acceleration the sectionalized collector was also used to determine the energy of the accelerated particles. In this case some of the sections were covered with aluminum foils of equal thickness (the method of filters). The measured relative activities of the sections covered by foils were compared with the computed values for different ion energies. The reaction yields for deuterons of initial energy E_0 that have passed through a filter of thickness d were computed from the formula

$$Y(E_0, d) = \int_0^{E_f} \frac{\sigma(E)}{\varepsilon(E)} dE,$$

where $\sigma(E)$ is the nuclear reaction cross section, $\varepsilon(E)$ is the stopping power of the filter material, and $E_f = f(E_0, d)$ is the energy of an ion that has passed through the filter. Calculations show that we can, in computing the reaction yield, neglect the fluctuations in the ionization losses in the filter material.

5. The proton-initiated reactions $^{12}C(p,\gamma)^{13}N$, $^{19}F(,\alpha\gamma)^{16}O$, and $^{14}N(p,\gamma)^{15}O$ proceed with the emission of prompt γ quanta. From the prompt-γ-ray signals we can extract information about both the proton-current-pulse shape and the characteristic proton velocity.[19] But the registration of prompt γ quanta entails some difficulties. In particular, it is necessary to separate the γ emission of the reaction from the bremsstrahlung of the relativistic electron beam. The energies of the γ quanta produced in the reactions $^{12}C(p,\gamma)^{13}N$ and $^{19}F(p,\alpha\gamma)^{16}O$ are respectively equal to 2.4 and 7.1 MeV, while the γ quanta of the bremsstrahlung have energies $\lesssim 1$ MeV. These two types of radiation are, in view of the appreciable difference in the energies of the γ quanta, attenuated differently by the shield surrounding the detector. Therefore, the use of a shield of optimal thickness raises the signal-to-noise ratio. Furthermore, the reception of the γ rays through a collimator and the use of thin targets, from which the bremsstrahlung yield is low, enable us to suppress the noise further.

In our first experiments we used a scintillation detector consisting of a plastic scintillator and an FÉU-54 photomultiplier. The thickness of the lead shield was 5–10 cm. The prompt γ radiation of the reaction $^{19}F(p,\alpha\gamma)^{16}O$ was received by the detector from a teflon target. But this reaction is inconvenient in that its yield strongly depends on the proton energy, and the current-pulse shape turns out to be distorted. The yield of the reaction $^{12}C(p,\gamma)^{13}N$ is practically independent of the proton energy, but it is significantly smaller in absolute value than the yield of the reaction on fluorine. Therefore, it has thus far not been possible to register the prompt γ rays of the reaction on carbon in ion-acceleration experiments.

It turned out to be possible to obtain a signal from a graphite target, as well as from a borne-nitride target, with the aid of the Cerenkov detector in which water was used as the radiator. As a result of the photoelectric effect, the Compton effect, or pair production, the

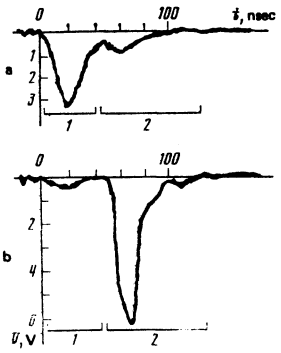

FIG. 3. Oscillograms of signals of the scintillation (a) and Cerenkov (b) detectors: 1) bremsstrahlung of the REB; 2) prompt γ radiation of the reaction $^{19}F(p, \alpha\gamma)^{16}O$.

γ quanta produce electrons in the water radiator. If the energy of the electrons is higher than 0.26 MeV, i.e., if their velocity is higher than the velocity of light in water, then Cerenkov radiation is generated which is registered by an FÉU-30 photomultiplier. At the same time, the major portion of the accelerator's bremsstrahlung (with quanta of energy lower than the indicated threshold energy) will not be registered. This leads to an appreciable increase in the signal-to-noise ratio. The time resolution of the Cerenkov detector of prompt γ rays is determined by the characteristics of the photomultiplier and the oscillograph. In our experiments it was ~5 nsec.

Figure 3 shows two oscillograms of prompt-γ-ray signals from a thick teflon target [the $^{19}F(p,\alpha\gamma)^{16}O$ reaction], which illustrate the advantages of the Cerenkov detector over the scintillation detector. The signals from the two detectors were obtained in one shot. The first peak on the oscillograms is due to the bremsstrahlung of the electrons, while the second peak corresponds to the prompt γ rays of the reaction. It can be seen that the Cerenkov detector significantly surpasses the scintillation detector in respect of the extent to which they are shielded from the bremsstrahlung noise.

6. For the measurement of the ion current we used several variants of the Faraday cylinder. A biased Faraday cylinder consisted of a case having an intake orifice of diameter 0.3 mm and a graphite collector inside it. To separate the ions from the accompanying electrons, a negative bias of several hundred volts was applied to the collector. Substantial errors can arise in the measurement of the ion current by such a cylinder because of secondary electron emission from the collector and the incidence on it of those electrons, accompanying the ions, whose energy exceeds the bias potential.[17]

The Faraday cylinder with a magnetic-field distortion practically does not have the disadvantage characteristic of the Faraday cylinder with a bias. The ions are received by a collector in the form of a cylinder cavity with an entrance orifice, in front of which a copper disk that distorts the magnetic field before it enters the collector is located. The characteristic scale of the field distortion is chosen such that the variation of the field is adiabatic for the electrons, but nonadiabatic for the

accelerated ions. As a result, a separation of the electrons from the ions occurs during their passage through the region of inhomogeneity of the magnetic field. The emission of secondary electrons from the collector is strongly suppressed, since these electrons move along the lines of force of the magnetic field, and only a small number of them can leave the collector through the intake orifice.

A Faraday cylinder records the ion-current density at a given point. The total ion current can be estimated on the basis of data on the current distribution over the cross section, which was determined from the radial profile of the target's activity. Moreover, the magnitude of the total ion current was computed from the known shape of the ion current and the total number of accelerated ions.

7. In order to determine the acceleration efficiency, i.e., the fraction of the REB energy transferred to the ions, we must know the number of accelerated particles and their energy spectrum. We determined the spectrum of the accelerated deuterons, using a time-of-flight neutron detector. The deuterons striking the graphite target produce neutron radiation as a result of the reaction $^{12}C(d,n)^{13}N(\beta^+)^{13}C$. The yield of this reaction increases sharply with increasing deuteron energy. This circumstance facilitates the registration of the deuterons in the high-energy part of the spectrum. The neutron detector was positioned at an angle $\theta_n = 120°$ with respect to the direction of motion of the deuterons reaching the target from the graphite. The distance between the detector and the target (the path length) $L = 4$ m. The neutrons were registered with the aid of recoil protons in a $3 \times 30 \times 30$-cm plastic scintillator. The scintillator was connected to a FÉU-30 photomultiplier by a light conductor. The detector was shielded from the hard bremsstrahlung of the accelerator by a lead sheet of thickness 7 cm. Figure 4 shows the oscillogram of a signal from the time-of-flight detector. After the first peak, (1), which is due to the x-bremsstrahlung of the accelerator, comes the signal, (2), due to the neutrons. Neutrons of energy $E_n \propto t^{-2}$ are registered at time t after the arrival of a deuteron at the target.

From the kinematics of the reaction it follows that the neutron energy (E_n) is connected with the deuteron energy (E_D) by the relation[20]

$$Q = \left(1 + \frac{m_n}{M}\right) E_n - \left(1 - \frac{m_D}{M}\right) E_D - \frac{2(m_n m_D E_D E_n)^{1/2}}{M} \cos\theta_n,$$

where $Q = -0.26$ MeV is the reaction energy; m_n and m_D are the neutron and deuteron masses; M is the mass of the isotope ^{13}N; θ_n is the angle between the directions of motion of the deuteron and neutron.

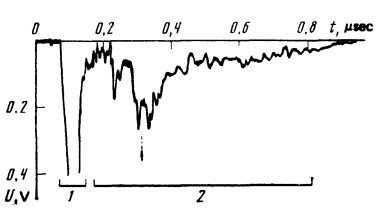

FIG. 4. Oscillogram of a signal from the time-of-flight neutron detector: 1) bremsstrahlung of the REB; 2) neutron signal.

The energy distribution of the deuterons, $dN_D(E_D)/dE_D$, was found from the relation

$$\frac{dN_D}{dE_D} = k \frac{dN_n}{dt} t^3 \varepsilon(E_n) \mu(E_n) Y^{-1}(E_D, \theta_n) F(E_D),$$

where dN_n/dt is the signal amplitude at the instant t; $\varepsilon(E_n)$ is the efficiency of registration of the neutrons by the detector; $\mu(E_n)$ is a coefficient taking account of the distortion of the neutron signal as a result of the slowing down of the neutrons in the shield; $Y(E_D, \theta_n)$ is the yield of the reaction; $F(E_D)$ is a coefficient allowing for the broadening of the neutron signal as a result of the slowing down of the deuterons in a thick target; and k is a numerical factor.

The neutron-registration efficiency, $\varepsilon(E_n)$, was computed by the method described by Egorov.[21] The dependence of the luminescence yield of the scintillator on the recoil-proton energy was taken into consideration in the computations. Since the slowing-down of the neutrons in the 7-cm-thick lead shield is slight, the coefficient $\mu(E_n)$ is close to unity. The reaction yield $Y(E_D, \theta_n)$ was computed from the data given in Refs. 22–24. The analysis of the broadening of the spectrum of the neutrons emitted by a thick target was performed in the same way as in Refs. 25 and 26. The absolute value of the $^{12}C(d,n)^{13}N$ reaction yield and the energy dependence of the yield are such that the neutron-spectrum broadening that arises as a result of the slowing down of the deuterons in the thick target is small; therefore, the factor $F(E_D) \approx 1$. The insignificant deviations of the factors $\mu(E_n)$ and $F(E_D)$ from unity were taken into consideration in computing the errors made in the determination of the energy distribution of the neutrons from the signal of the time-of-flight detector.

The data were analyzed with allowance for the contribution to the neutron signal (for $E_D \gtrsim 2.4$ MeV) from the reaction involving the production of the isotope ^{13}N in the excited state,[27] as well as for the insignificant (~5%) contribution from the neutrons with $E_n \gtrsim 5$ MeV produced in the reaction $^{13}C(d,n)^{14}N$. The nautral percentage of the isotope ^{13}C in graphite is ~1%. The cross section for the reaction $^{13}C(d,n)^{14}N$ is given in Ref. 22. The main source of errors in the determination of the neutron, and, consequently, deuteron, spectrum is some uncertainty in the arrival time of the deuteron at the target (the choice of zero time in the time-of-flight measurements). Under our conditions the error made in the reckoning of this time was largely determined by the duration of the REB, and was $\lesssim 40$ nsec.

Thus, the measurement of the neutron spectrum for the reaction $^{12}C(d,n)^{13}N$ allows us to determine the spectrum of the deuterons of energy $E_D \gtrsim 0.5$ MeV with a high degree of certainty.

8. Data on the composition of the ion flux and the energy distribution of the accelerated ions in a broad energy range were obtained with the aid of an electrostatic analyzer with a nuclear photoemulsion as the

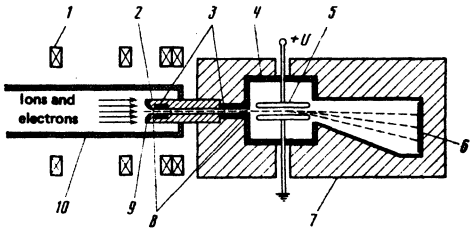

FIG. 5. Diagram of the electrostatic ion analyzer: 1) solenoid, 2) copper cylinder, 3) tantalum diaphragm, 4) analyzer casing, 5) deflecting plates, 6) nuclear photoemulsion, 7) lead shield, 8) collimator slits, 9) graphite absorber, and 10) drift chamber.

detector. These data, together with the results of the determination of the number of accelerated ions by the activation methods, enable us to obtain complete information about the energy characteristics of the ion flux.

A diagram of the electrostatic analyzer is shown in Fig. 5. The particles to be analyzed pass through a collimator consisting of two 2×0.5-mm slits located at a distance of 25 cm from each other. After the collimator the particles enter a transverse electric field between deflecting plates, and, at 28 cm from these plates, are registered by a nuclear photoemulsion. The nuclear photoemulsion allows us to reliably identify the registered particles by their tracks. The intensity of the analyzing electric field was varied in the range $0 \leq E \leq 15$ kV/cm. The potential difference between the plates was controlled over the duration of the acceleration pulse with the aid of a divider. To shield the photoemulsion from the hard bremsstrahlung of the accelerator, the analyzer was placed in a lead screen, and the parts of the collimator were fabricated from tantalum.

The ions propagate together with the electrons, neutralizing their space charge. In order to analyze the ions in the electric field, we must separate them from the accompanying electrons. This separation was accomplished by passing the electron-ion flux through a region of rapid variation of a magnetic field. To realize the required magnetic-field configuration, the first slit of the collimator was imbedded in a solid copper cylinder of diameter 5 cm. Because of the skin effect, the magnetic field at the center of the cylinder was more than two orders of magnitude weaker than the external field. To secure the most rapid variation of the magnetic field over a minimal distance (characteristic scale ~1 cm), a special profile was chosen for the cylinder as viewed from the incident beam. On entering the cylinder, the electrons are separated from the ions, and run off along the lines of force to a graphite absorber. The dimensions of the collimator and the magnetic-field configuration were such that the distortion of the ion spectrum as a result of the electrostatic repulsion of the ion beam and the passage of the ions through the magnetic field jump was negligible. The measurement results were processed under the assumption that ions with different energies have the same angular spread.

The ion current that passed through the collimator could be registered with the aid of a Faraday cylinder mounted either directly behind the plates or at a distance of 60 cm from them (corresponding to distances of 125 and 185 cm from the foil anode of the accelerator).

III. EXPERIMENTAL RESULTS

One of the basic problems that were solved in the experiments consists in the determination of the optimal conditions for the acceleration of ions. By optimal conditions is meant those conditions under which the highest coefficient of energy transfer from the REB to the accelerated-ion flux is attained. The second important problem was to determine the principal characteristics of the ion flux produced under the optimal conditions.

1. *Optimization.* To find the optimal ion-acceleration regime, we varied the following parameters in the experiment: the material and thickness of the foil anode 5 and the dielectric film 6 (see Fig. 2), the distance between them, the distance between the cathode and the foil anode 5, and the strength of the longitudinal magnetic field. As the foil anode we used aluminum of thickness from 6 to 20 μm and aluminized "kimfol" of thickness from 2 to 8 μm; as the dielectric film we used polyethylene $(CH_2)_n$, "kimfol" $(C_{12}H_{14}O_3)_n$, polypropylene $(CH_2)_n$, and lexan $(C_{10}H_8O_4)_n$ of thickness from 2 to 40 μm.

The experiments showed that the efficiency with which energy is transferred to the ion flux increases rapidly as the total thickness of the anode foils is decreased, but weakly depends on the material of the dielectric films. Therefore, in the majority of the experiments we used foils with the smallest possible thickness (2 μm). If, on the other hand, we used as the foil anode 5, for example, 9-μm-thick aluminum, then the acceleration efficiency decreases by roughly a factor of three. This fact can be qualitatively explained as follows. The electrons oscillating near the foils lose energy in the foils at the same time as they cool down as a result of the transfer of their energy to the accelerated ions.[6] To these two processes correspond the following characteristic oscillation times, expressed in terms of the number of electron transits: $N_1 \sim E/\delta E$ and $N_2 \sim c/v_i$, where E is the initial electron energy, δE is the energy lost by an electron in a single transit through the anode foils, and v_i is the characteristic velocity of the accelerated ions. For the acceleration to be effected efficiently, the electrons should transfer their energy to the ions more rapidly than they lose energy in the anode foils, i.e., the condition $N_1 > N_2$ should be fulfilled. Estimates show that this condition is fulfilled at total aluminum-foil thicknesses less than ~10 μm.

A change of the distance between the cathode and the foil anode from 10 down to 4 mm leads to a roughly fivefold increase in the number of accelerated ions. When the diode gap is reduced, the magnitude of the electric-field intensity in the diode increases. As a result, the shutoff of the diode by the space charge of the electron cloud occurs at a higher oscillating-electron density. As follows from Stupakov's investigation,[6] the density of the accelerated ions is proportional to

that of the gathered electrons; consequently, the acceleration regime with the smallest diode gap, to which corresponds the highest electron density in the cloud, should be the most effective. The smallest possible distance between the cathode and the foil anode is determined by the operational stability of the diode. The probability of a breakdown of the diode gap increases as the gap is decreased. It was experimentally established that the operational stability of the diode rises if the aluminized "kimfol" foil has its dielectric surface facing the cathode. This circumstance has also been noted by Bystritskii and Krasik.[28]

The acceleration efficiency is significantly affected by the distance between the foil anode 5 and the dielectric film 6, as well as by a thin aluminum ring of inside diameter equal to the electron-beam diameter, pressed against the surface of the dielectric film. There exists for the width of the gap between the foils some optimum value at which the highest number of accelerated protons is recorded. The optimum distance between the foils is determined by both the process of plasma production at the surface of the dielectric film and the position of the plasma relative to the potential well formed by the oscillating electrons.

The ion-acceleration efficiency weakly depends on the magnetic-field intensity, H_0, in the range from 5 to 20 kOe. The number of accelerated ions drops sharply when the field intensity is decreased to $H_0 \lesssim 30$ kOe. Estimates show that the gas-dynamical pressure of the electron cloud is comparable to the pressure of the external magnetic field when $H_0 \sim 3$ kOe. In a weaker field, the electron cloud expands in the transverse direction. This leads to the loss of some of the oscillating electrons and the decrease of the acceleration efficiency.

Thus, as a result of the experiments, we have established the following conditions for the most efficient acceleration of ions by a cloud of relativistic electrons. In the optimum acceleration regime the distance between the cathode and the foil anode was 5 mm for a cathode diameter of 30 mm. The foil anode was a 2-μm-thick aluminized "kimfol" with the dielectric surface facing the cathode. As the dielectric film we used kimfol of thickness 2 μm. The distance between the foil anode and the dielectric film was 4 mm. The strength of the longitudinal magnetic field exceeds 5 kOe in the optimum regime.

2. *Performance of the diode.* The performance characteristics of the diode under optimum acceleration conditions are illustrated in Fig. 6. The single-transit regime for the electrons is realized if a graphite collector is located directly behind the foil anode to receive the electron beam (Fig. 6, the curves 1). In this case a cloud of oscillating relativistic electrons is not formed, and there is no space charge to cause a shut off of the diode. The shape of the diode current roughly duplicates that of the voltage. The voltage on the cathode rises within 5 nsec to 1 MV, and then decreases to zero in ~60 nsec. The diode current strength attains a value of $I_d \approx 20$ kA.

In the ion-acceleration regime (Fig. 6, the curves 2),

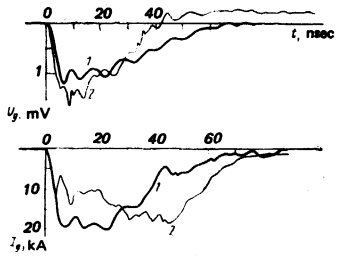

FIG. 6. Oscillograms of the diode voltage U_d and of the diode current I_d: 1) regime of single transit of the REB through foil anodes; 2) ion-acceleration regime.

there occurs a partial shut off of the diode under the action of the space charge of the relativistic-electron cloud. During the first 20 nsec the diode current is equal to $I_d \approx 10$ kA, and the magnitude of the voltage is slightly greater than the magnitude in the single-transit regime. After the shut off phase, the diode current beings to rise. The increase of the current is apparently due to the filling of the diode by ions and/or the motion of the anode plasma. This effect was observed in, for example, experiments on the "INAR" facility.[29] The magnitude of this rise in the diode current can vary from one discharge to another, but the number of accelerated ions varies insignificantly in the process.

In the ion-acceleration regime, the total current in the drift chamber was measured with the aid of a Rogowski loop and a shunt in the collector circuit. A vacuum current of strength significantly less than the diode current is registered in the chamber at the beginning of the REB injection. The oscillograms of this current exhibit intense oscillations, the mean vacuum current strength being equal to 2–3 kA. In due course, as a result of the formation and propagation of the ion flux in the drift chamber, the total current becomes nearly equal to zero, which may indicate the neutralization of the electron beam by the ions.

3. *The ion current.* The shape of the ion-current pulse received by the collector was determined from the prompt γ emission of the nuclear reactions. In Fig. 7, (b–d) we show oscillograms of prompt-γ-radiation signals from a teflon film of thickness 20 μm loca-

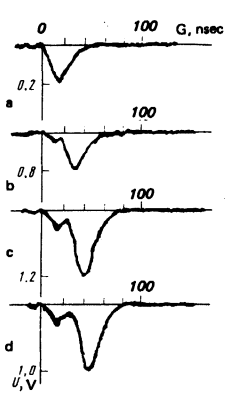

FIG. 7. Oscillograms of γ-radiation signals from a fluoroplastic film located at different distances z from the foil anode: b) $z = 40$ cm; c) $z = 50$ cm; d) $z = 60$ cm; a) bremsstrahlung of the REB.

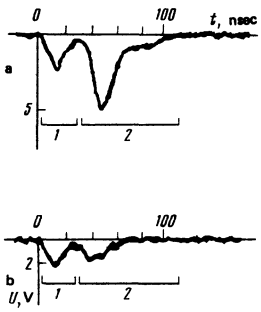

FIG. 8. Oscillograms of γ-radiation signals for a fixed distance of 60 cm between the foil anode and the collector and different targets: a) C (graphite); b) BN (boron nitride). 1) Bremsstrahlung of the REB, 2) prompt γ radiation.

ted at distances of 40, 50, and 60 cm, respectively, from the foil anode. The first oscillogram [Fig. 7(a)] depicts the bremsstrahlung of the REB. In the following oscillograms [Figs. 7(b)–7(d)], after the bremsstrahlung pulse comes a signal due to the γ radiation from the reaction $^{19}F(p, \alpha\gamma)^{16}O$. The yield of this reaction, which has a threshold of 0.227 MeV, increases with increasing proton energy,[19] which improves the registration conditions for high-energy protons. The highest energy of the registered protons, as estimated from the time-of-flight measurements, is ~2 MeV.

In Fig. 8 we show oscillograms of prompt γ-radiation signals from a carbon target (a) and a boron-nitride target (b). These signals correspond to a current of protons of energies higher than 0.47 MeV (C target) and 1.06 MeV (BN target). The current-pulse duration for the protons of energies higher than 0.47 MeV is ~80 nsec at a distance of 60 cm from the foil anode. A time-of-flight analysis of the prompt-γ-radiation signals shows that the instantaneous velocity of the protons arriving at the target exceeds their mean velocity over the length of the setup. This is explained by the fact that the ions are accelerated in an interval of time comparable to the REB duration (~50 nsec), and, as shown earlier,[13] the characteristic scale for the ion acceleration is several tens of centimeters.

Figure 9 shows ion-current signals obtained with Faraday cylinders located at different distances from the foil anode of the accelerator. The ion-current density registered at $z = 60$ cm attained a value of 400 A/cm^2.

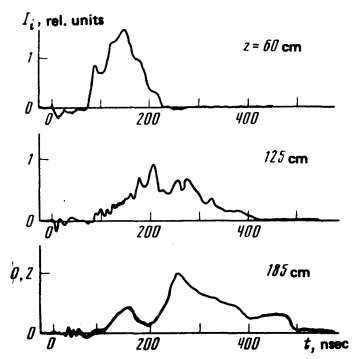

FIG. 9. Oscillograms of ion-current signals from the Faraday cylinder at different distances from the foil anode.

Estimates of the total ion current yield a value $I_i = 3-4$ kA. Let us compare the shape of the ion current at $z = 60$ cm with the shape of the prompt-γ-radiation pulse (see Fig. 8). The signal from the Faraday cylinder appears about 40 nsec after the appearance of the γ-radiation signal. This happens because for ~70 nsec the ion current is neutralized by fast electrons. In the case of a grid bias of 300 V the fast electrons cannot be separated from the ions, and therefore the registrable current is equal to zero. Subsequently, the characteristic energy of the neutralizing electrons is $\lesssim 100$ eV. These slow electrons are split off by the bias potential, and the detector registers an ion current. For large distances ($z = 125$, 185 cm), the ion flux propagates for a time > 70 nsec, and therefore the instant at which the ion current starts in these oscillograms characterizes the time of flight of the protons from the foil anode to the detector. The characteristic energy of these protons is ~1.5 MeV. The duration of the ion current exceeds that of the prompt-γ-radiation pulse. From this it can be concluded that a significant part of the accelerated protons have energies smaller than 0.47 MeV (the threshold energy for the appearance of the prompt γ radiation). At large z the duration of the ion current significantly exceeds the ion-beam-production time; consequently, the shape of the ion-current pulse (under the assumption of a homogeneous mass composition) reflects the energy distribution of the ions (see Fig. 9, $z = 125$, 185 cm). Time-of-flight estimates show that the proton energies range roughly from 100 keV to 1.5 MeV.

4. *Energy distribution and composition of the ion flux.* More accurate data on the energy distribution of the accelerated ions and the composition of the ion flux were obtained with the aid of an electrostatic analyzer. Figure 10 shows an image of the track of an ion beam in a nuclear photoemulsion after the particles had passed through the deflecting electric field. The neutral particles are registered at the point $X = 0$ (without deflection in the electric field); the blackening of the photoemulsion at this place is appreciable. The emulsion blackening at $X > 0$ is produced by ions. It can be seen from the figure that a photoemulsion registers a broad

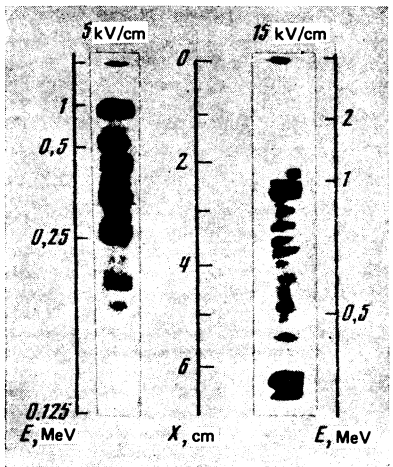

FIG. 10. Track of the ion beam in a nuclear photoemulsion.

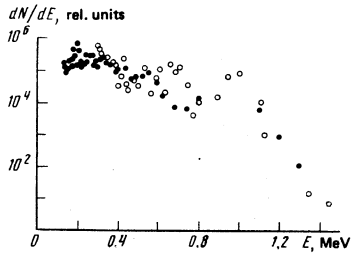

FIG. 11. Accelerated-proton spectra for different analyzing electric field intensities; ●) 5 kV/cm; ○) 10 kv/cm.

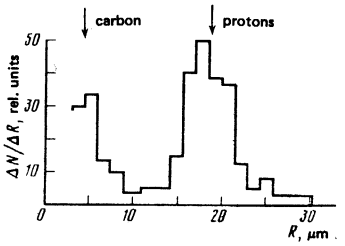

FIG. 12. Range distribution of the ions in a nuclear photoemulsion (for a fixed energy of 1.5 MeV).

ion spectrum with a complex discrete structure. The "modulation" index of the energy distribution of the ions attains a value of 100%. The X distribution of the number of ions was determined by counting the number of tracks under a microscope. The track shape and length (the range of the particles in the photoemulsion) could also be observed by depth scanning the photoemulsion. In a number of experiments the photoemulsion was mounted at an angle of 45° to the direction of propagation of the ions. The length and shape of the tracks could be determined with greater accuracy in this case.

The proton energy determined from the range in the photoemulsion at fixed particle deflection along the X-coordinate axis is equal to the computed value. The deflection of the ions along the X axis is inversely proportional to their energy ($X \propto 1/E$). By counting the tracks of the protons, we can determine the spectrum of these particles:

$$\frac{dN(E)}{dE} \propto X^2 \frac{dN(X)}{dX}.$$

The proton spectra for two typical discharges are shown in Fig. 11. The error in the determination of the spectrum is primarily due to the finite energy resolution of the analyzer ($\delta E/E \lesssim 10\%$) and the statistical error in the counting of the tracks ($\Delta N/N \lesssim 10\%$). The spread of the points on the spectrum (modulation of the spectrum) is a property of the spectrum. As can be seen from the data presented, a large group of the accelerated protons have a characteristic energy ~0.3 MeV; at the same time there are a considerable number of particles with energy ~1 MeV. The highest energy of the protons registered with the aid of the analyzer is ~2 MeV.

The determination of the number of accelerated protons with the aid of the activation technique, together with the measurements of the proton spectrum allows us to determine the energy distribution of the accelerated particles on the absolute scale. The number of protons with energies higher than 0.47 MeV, as computed from the carbon-target-activation measurements was as high as 5.5×10^{14} particles per pulse. The integration of the spectrum, normalized to these data, over the energy range from 0.1 to 2 MeV yields for the total number of accelerated protons per pulse a value equal to $(2 \pm 0.5) \times 10^{15}$ particles. The calculated values for the number of particles of energy $E_p > 0.27$ MeV contained in the spectrum agree with the results of the determination of this quantity by the method of proton activation of a boron-nitride target. Analysis of the obtained energy distribution of the protons shows that the ion-current signal (see Fig. 9) is due largely to protons. Therefore, we can estimate the highest ion current, knowing the shape of this current and the total number of protons. The strength of the current at a distance of 60 cm from the foil anode was as high as 3.5 ± 0.5 kA.

From the spectrum of the particles we can find the spectral distribution, $E\Delta N/\Delta E$, of the energy of the accelerated-ion flux. About half of the energy of the accelerated-ion flux is carried by the particles with energy lower than 0.5 MeV. A significant fraction of the total energy is held by particles with characteristic energy ~1 MeV. The total energy carried by the proton beam is equal to

$$Q_p = \int_0^\infty E \frac{\Delta N}{\Delta E} dE = 130 \pm 30 \text{ J}.$$

(The error in the determination of the total energy is due largely to the error in the measurement of the ion spectrum.)

The recording of the shape and length of the particle tracks in the photoemulsion allows us to detect heavier particles along with the protons. Figure 12 shows the range distribution, $\Delta N/\Delta R$, of the ions in the nuclear photoemulsion for an ion energy equal to 1.5 MeV (fixed X coordinate). In this case the statistics were collected by moving the photoemulsion in the direction perpendicular to the X axis. The range distribution exhibits two peaks. The arrows in the figure indicate the tabular range values for protons and carbon ions with energy 1.5 MeV. Therefore, the peak with the characteristic value ~20 μm is identified with protons, while the peak in the smaller-range region is identified with heavy ions with atomic weights $A = 12-16$. Evidently, this peak corresponds to carbon ions ($A = 12$), since the dielectric film serving as the ion source consists primarily of hydrogen and carbon. The given uncertainty in the atomic weight is due to the error in the measurement of the range of the ions in the photoemulsion. In the region of small ranges ($\lesssim 5$ μm), the measurement error can be as high as 50%. This spread of the measured ranges is determined by both the precision of the microscope ($\Delta R_m \approx 1.0$ μm) and the energy resolution of the analyzer. The number of accelerated heavy ions can be determined by counting the number of proton and heavy-ion tracks. This is possible for heavy ions with energy higher than 1 MeV. At lower energies the lengths of the heavy-ion tracks become comparable to the dimension of a grain in the photoemulsion (~0.5 μm), and the measurement of the track lengths becomes dif-

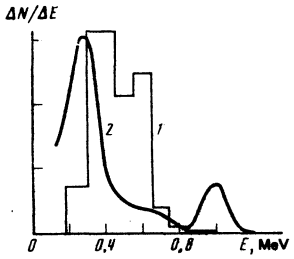

FIG. 13. Spectra of the hydrogen atoms (1) and the protons (2).

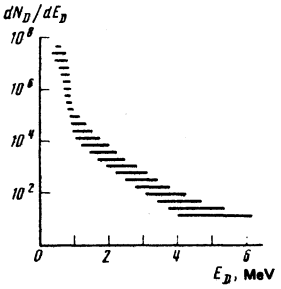

FIG. 14. Spectrum of the accelerated deuterons.

ficult. In the region of energies $E > 1$ MeV, the number of heavy ions (carbon ions) constitutes ~20% of the total number of ions.

Another variety of tracks is observed in the nuclear photoemulsion. They are double tracks ("forks") originating from one point, and having a length equal to half the length of the proton track for the same energy. The measurement of the lengths of, and the angles between, these tracks enabled us to identify them as the tracks of protons produced upon the dissociation in the photoemulsion of H_2^+ ions. The number of H_2^+ ions constitutes ~ 1% of the total number of ions, and the energy spectrum roughly corresponds to the proton spectrum.

Some of the accelerated particles pass through the electric field region in the analyzer without being deflected. These are neutral particles. The energy distribution of the neutral particles, obtained from the tracks in the nuclear photoemulsion, is shown in Fig. 13, the curve 1. For comparison, the proton spectrum is shown in the same figure (the curve 2). It can be seen that most of the neutral particles have energies ~0.5 MeV, the number of particles with energy higher than 1 MeV being negligibly small. The number of neutral particles also constitutes ~1% of the total number of accelerated ions. Their tracks are similar to the proton tracks. Evidently, these are neutral H atoms, which are produced as a result of the dissociation of H_2^+ ions by the residual gas in the drift chamber.

This composition of the ion flux can be explained as follows. The oscillating relativistic electrons produce at the surface of the dielectric film a plasma consisting of protons, H_2^+ ions, and heavy (carbon) ions. The ions of this plasma are accelerated at the expense of the energy of the relativistic electrons. In the course of the acceleration, some of the H_2^+ ions dissociate as a result of collisions with the molecules of the residual gas into either two protons or a proton and a hydrogen atom. The hydrogen atom subsequently retains an energy equal to half the energy of the H_2^+ ion at the moment of dissociation, while the proton may be further accelerated.

Let us briefly discuss the results of the experiments on the acceleration of deuterium ions. A deuteron beam can be obtained if the dielectric film is thinly coated with deuterated polyethylene $(CD_2)_n$. The total number of radioactive ^{13}N produced in the reaction $^{12}C(d,n)^{13}N(\beta^+)^{13}C$, like the number of emitted neutrons, which was measured by a neutron-activation detector, was 10^8 per pulse. The accelerated-deuteron spectrum, which was obtained with the aid of a time-of-flight neutron detector, is shown in Fig. 14. As has already been noted, this detector possesses a high sensitivity in the high-energy region. We succeeded in establishing with its aid that the spectrum contains deuterons with energies right up to 4–6 MeV. Measurements performed with the aid of the method of filters also showed that a significant part of the deuterons have energies exceeding the energy of the electrons of the REB. The shape of the deuteron spectrum in the low-energy region qualitatively agrees with that of the accelerated-proton spectrum. Most of the deuterons have energies $\lesssim 1$ MeV. The number of deuterons with energies higher than ~0.5 MeV is $\sim 10^{14}$ particles per pulse (the deuterons were accelerated under conditions not corresponding to the optimum conditions). The measurements of the radial profile of the graphite target's activity showed that the transverse dimension of the deuteron beam insignificantly exceeds the diameter of the REB. The angular divergence of the beam produced was 2–3°.

5. *The energy balance.* Let us consider the energy balance in the optimum acceleration regime. The total energy of the accelerated-ion flux is equal to $Q_i = 130 \pm 30$ J. The energy of the injected electron beam

$$Q_b = \int U_d I_d dt = 350 \text{ J},$$

where U_d and I_d are the diode voltage and current. A portion of this energy is carried away by the vacuum current:

$$Q_{vac} = \int U_d I_{vac} dt \approx 70 \text{ J}.$$

We can now determine the acceleration efficiency, i.e., the fraction of the energy that is transferred to the ions by the electron cloud. In our experiments this efficiency is

$$\eta = Q_i/(Q_b - Q_{vac}) = 47 \pm 13\%.$$

The efficiency attained in the ion acceleration is comparable to the acceleration efficiency achieved in such "direct" methods as those employing reflecting systems,[30] magnetically insulated diodes,[31,32] and diodes with a pinched electron beam.[33] At the same time the efficiency of the collective gas-dynamical acceleration is significantly higher than the efficiencies of the other methods of collective acceleration of ions.[8,9,34,35]

Thus, as a result of the experiments performed, we have found the physical conditions under which ~50% of the energy stored in the oscillating electron cloud is

transferred to the accelerated ions. Analysis of these conditions shows that the formation of the densest relativistic-electron cloud and the efficient production of a surface plasma layer correspond to the optimum acceleration regime for the ions.

New diagnostic methods have been developed for the measurement of the characteristics of the ion flux. It has been found that the accelerated-ion flux has a broad energy spectrum. Most of the accelerated ions have energies comparable to the energy of the relativistic electrons (~ MeV). Some of the ions acquire energies significantly higher than the energy of the injected electrons. The number of accelerated ions can be as high as 2×10^{15} particles per pulse in the case in which the total number of electrons in the REB is $\sim 4\times 10^{15}$. The highest ion current at a distance of 60 cm from the foil anode of the accelerator is 3.5 kA for a diode current ~10 kA. The ion flux consists of protons (or deuterons), as well as heavy ions, depending on the composition of the dielectric film in the anode unit of the accelerator.

The authors express their sincere gratitude to D. D. Ryutov for attention to the work and for numerous useful discussions, A. V. Arzhannikov and V. V. Konyukhov for their help in the performance of the experiments, and V. P. Smakhtin and Yu.A. Tikhonov for their assistance in the application of the nuclear diagnostic methods.

[1)]The method of producing a plasma layer through the ionization of a dielectric under the action of a relativistic-electron beam was first used by Humphries *et al.*[11]

[1]J. M. Creedon, I. D. Smith, and D. S. Prono, Phys. Rev. Lett. **35**, 91 (1975); D. S. Prono, J. M. Creedon, I. D. Smith, and N. Bergstrom, J. Appl. Phys. **46**, 3310 (1975).
[2]D. D. Ryutov and G. V. Stupakov, Fiz. Plazmy **2**, 566 (1976) [Sov. J. Plasma Phys. **2**, 309 (1976)].
[3]A. V. Arzhannikov, A. V. Burdakov, V. S. Koĭdan, and D. D. Ryutov, Pis'ma Zh. Eksp. Teor. **24**, 19 (1976) [JETP Lett. **24**, 15 (1976)].
[4]D. D. Ryutov and G. V. Stupakov, Fiz. Plazmy **2**, 767 (1976) [Sov. J. Plasma Phys. **2**, 427 (1976)].
[5]D. D. Ryutov, Preprint Inst. Yad. Fiz. Sibirsk. Otd. Akad. Nauk SSSR, 77–4, Novosibirsk, 1977.
[6]G. V. Stupakov, Preprint Inst. Yad. Fiz. Sibirsk. Otd. Akad. Nauk SSSR, 80–93, Novosibirsk, 1980; Fiz. Plazmy **6**, 1322 (1980) [Sov. J. Plasma Phys. **6**, 724 (1980)].
[7]J. A. Nation, Particle Accelerators, **10**, 1 (1979).
[8]K. L. Olson, Fiz. Plazmy **3**, 465 (1977) [Sov. J. Plasma Phys. **3**, 259 (1977)].
[9]V. G. Gapanovich and A. A. Kolomenskiĭ, Izv. Vyssh. Uchebn. Zaved. Fiz. **10**, 59 (1979).
[10]V. M. Bystritskiĭ, Izv. Vyssh. Uchebn. Zaved. **10**, 83 (1979).
[11]S. J. Humphries, Y. G. Lee, and R. N. Sudan, Appl. Phys. Lett. **25**, 20 (1974).
[12]J. Golden and C. A. Kapetanakos, Appl. Phys. Lett. **28**, 3 (1978).
[13]A. V. Burdakov, V. V. Chikunov, V. S. Koidan, and A. I. Rogozin, Proc. Third Intern. Topical Conf. on High-Power Electron and Ion Beam Research and Technology, Novosibirsk, 1979, Vol. 1, p. 315.
[14]A. V. Burdakov, V. S. Koĭdan, A. I. Rogozin, and V. V. Chikunov, Pis'ma Zh. Eksp. Teor. Fiz. **31**, 100 (1980).
[15]F. C. Young, J. Golden, and C. A. Kapetanakos, Rev. Sci. Instrum. **48**, 432 (1977).
[16]A. E. Blaugrund and S. J. Stephanakis, Rev. Sci. Instrum. **49**, 866 (1978).
[17]C. Eichenberger, S. Humphries, J. Maenchen, Jr., and R. N. Sudan, J. Appl. Phys. **48**, 1449 (1977).
[18]A. O. Hanson and J. L. McKibben, Phys. Rev. **72**, 673 (1947).
[19]J. Golden, R. A. Mahaffey, J. U. Pasour, F. C. Young, and C. A. Kapetanakos, Rev. Sci. Instrum. **49**, 1385 (1978).
[20]N. A. Vlasov, Neĭtrony (Neutrons), Nauka, Moscow, 1971.
[21]Yu. A. Egorov, Stsintillyatsionnyĭ metod spektrometrii gamma-izlucheniya i bystrykh neĭtronov (The Scintillation Method of Gamma-Radiation and Fast-Neutron Spectrometry), Gosatomizdat, Moscow, 1963.
[22]R. J. Jaszczak *et al.*, Phys. Rev. **181**, 1428 (1969).
[23]J. R. Davis and G. U. Din, Nucl. Phys. A **179**, 101 (1972).
[24]A. Elwin *et al.*, Phys. Rev. **116**, 1490 (1959).
[25]F. S. Young, D. Mosher, S. J. Stephanakis, S. Goldstein, and D. Hisshelwood, NRL Memorandum Report 3823, 1978.
[26]H. H. Anderson and J. F. Ziegler, The Stopping and Ranges of Ions in Matter, Vol. 3, New York, 1977.
[27]J. R. Sawers, Phys. Rev. **141**, 825 (1966).
[28]V. M. Bystritskiĭ and Ya. E. Krasik, Fiz. Plazmy **6**, 413 (1980).
[29]A. V. Arzhannikov and V. S. Koĭdan, Preprint Inst. Yad. Fiz. Sibirsk. Otd. Akad. Nauk SSSR, 80–73, Novosibirsk, 1980.
[30]J. A. Pasour, R. A. Mahaffey, J. Golden, and C. A. Kapetanakos, Appl. Phys. Lett. **36**, 646 (1980).
[31]R. N. Sudan and R. V. Lovelace, Phys. Rev. Lett. **31**, 1174 (1973).
[32]S. J. Humphries, R. N. Sudan, and L. G. Wiley, J. Appl. Phys. **47**, 2382 (1976).
[33]A. E. Blaugrund and G. Cooperstein, Phys. Rev. Lett. **34**, 461 (1975).
[34]O. Zucker, J. Wyatt, H. Sahlin, J. S. Luse, B. Freeman, and R. Gullickson, Proc. Third Intern. Conf. on Collective Method of Acceleration, Univ. of California, Irvine, 1978.
[35]A. A. Kolomenskiĭ, V. M. Likhachev, I. V. Sinil'shchikova, O. A. Smit, and V. N. Ivanov, Zh. Eksp. Teor. Fiz. **68**, 51 (1975) [Sov. Phys. JETP **41**, 26 (1975)].

Translated by A. K. Agyei